RESEARCH ARTICLE | JULY 13 2023

Effects of different current confinement layers in GaN-based VCSELs

Yan-Hui Chen ; Yang Mei ; Zhong-Ming Zheng ; Rong-Bin Xu ; Ya-Chao Wang ; Lei-Ying Ying ; Zhi-Wei Zheng ; Hao Long ; Yi-Kun Bu ; Bao-Ping Zhang

AIP Advances 13, 075114 (2023)
https://doi.org/10.1063/5.0155159

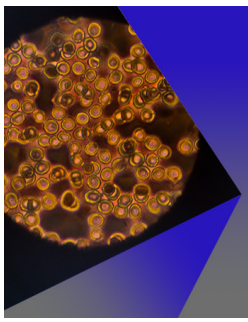

Effects of different current confinement layers in GaN-based VCSELs

Cite as: AIP Advances 13, 075114 (2023); doi: 10.1063/5.0155159
Submitted: 18 April 2023 • Accepted: 29 June 2023 •
Published Online: 13 July 2023

Yan-Hui Chen, Yang Mei,[a] Zhong-Ming Zheng, Rong-Bin Xu, Ya-Chao Wang, Lei-Ying Ying, Zhi-Wei Zheng, Hao Long, Yi-Kun Bu, and Bao-Ping Zhang[a]

AFFILIATIONS

Department of Microelectronics and Integrated Circuit, School of Electronic Science and Engineering, Xiamen University, Xiamen 361005, China

[a]Authors to whom correspondence should be addressed: meiyang@xmu.edu.cn and bzhang@xmu.edu.cn

ABSTRACT

For GaN-based vertical-cavity surface-emitting lasers (VCSELs), a suitable current confinement layer is essential for high-performance devices. The effect of different current confinement layers, including SiO_2, AlN, and diamond, on the performance of GaN-based VCSELs was compared through simulation. The devices' heat dissipation and current confinement characteristics were analyzed based on the electro-opto-thermal model. Considering thermal management, the diamond was a better candidate under high injected current. Benefiting from the excellent heat dissipation, the device with diamond shows a significant improvement in output power and the thermal roll-over current. This work gives a superior option for the current confinement layer and can be helpful for future design and fabrication of high-power GaN-based VCSELs.

I. INTRODUCTION

GaN-based vertical-cavity surface-emitting lasers (VCSELs) have attracted significant attention in recent years due to their excellent optical and electrical characteristics, such as low threshold current, narrow linewidth, high brightness, and excellent directionality.[1,2] These properties make them ideal light sources in applications such as optical communication, 3D sensing,[3] and especially in the new boosting VR/AR systems.[4] With gratitude to the researchers' outstanding dedication and the development of GaN-based material, lasing of GaN-based VCSELs covering from ultraviolet to yellow-green has been demonstrated.[5–9] At present, optimizing the performance of GaN-based VCSELs under high injection current has become more critical and attracted much attention.

The dual dielectric Distributed Bragg Reflector (DBR) structure and the hybrid DBR structure are the two mainstream structures of GaN-based VCSELs.[6,10–13] The former has both top and bottom DBRs deposited with dielectric materials, while the latter has a bottom nitride DBR and a top dielectric DBR. The dual dielectric DBR structure can avoid the difficulties in epitaxial nitride DBRs, including the narrow stop band, low reflectivity, and long MOCVD growth time,[14] which can help to realize a lower threshold current. However, self-heating is more severe in the device with the dual dielectric DBR structure, especially in the device with a short cavity, because the thermal conductivity of the dielectric bottom DBR is extremely low (SiO_2 ~ 1.5 W/mK, ZrO_2 ~ 2.09 W/mK, TiO_2 ~ 6.5 W/mK).[15–18] When the device works under high current, the influence caused by high device temperature is essential. Serious self-heating can cause degradation in the device performance, including the threshold current, the output power, and the emission spectrum.[19–22]

Several methods have been investigated to optimize the heat dissipation in devices with this structure. Mishkat-Ul-Masabih *et al.* from UNM[23] and Mei *et al.* from XMU[18] proposed that increasing the cavity length can improve the heat dissipation. Mehta *et al.* from Georgia Tech[24] proposed to broaden the substrate diameter and reduce the diameter of the p-side DBR to improve the heat dissipation. Leonard *et al.* from UCSB,[25] as well as our previous studies,[5] reported that transferring the device membrane to a bonded copper plate can effectively improve the heat dissipation. Benefiting from the improved heat dissipation performance, we have experimentally improved the device performance in our previous studies.[8,12]

According to the thermal analysis on GaN-based VCSELs performed by Mei *et al.*,[18] the vertical transfer of the heat generated in

the active region directly through the bottom DBR is obstructed. It is caused by the low thermal conductivity of the bottom dielectric DBR. Therefore, the heat needs to be transported laterally, bypassing the bottom DBR, and then transported vertically to the heat sink, as shown in Fig. 1. The current confinement layer is located at the main pathway of thermal transport, which will influence the heat dissipation in devices. Therefore, choosing a material with a higher thermal conductivity as the current confinement layer can significantly improve the heat dissipation of the devices.

Due to the mature fabrication process, the most commonly used material of the current confinement layer is SiO_2.[10,13,26] However, the thermal conductivity of SiO_2 is extremely low (~1.5 W/mK), which will seriously restrict heat dissipation. In our previous work, we utilized AlN (thermal conductivity ~200 W/mK) to replace SiO_2, and improved experimental results were obtained. With a steady-state quasi-3D heat dissipation model,[27] better heat dissipation was demonstrated. However, it is not clear whether the performance of the device can be further improved with an even better thermal-conducting confinement layer. Furthermore, analyzing the device systematically by an electro-opto-thermal model should be highly desired.

In this study, an electro-opto-thermal model was built, and the performance of devices using SiO_2, AlN, and diamond as current confinement layers, respectively, was compared. Diamond has a much higher thermal conductivity than AlN (diamond ~ 2200 W/mK).[28] The thermal resistance of the devices decreased from 719.15 to 438.3 K/W (an improvement of 39%) when the current confinement layer was changed from SiO_2 to AlN. Because the thermal conductivity of the diamond is higher than that of the AlN, utilizing the diamond as the current confinement layer can further decrease the device's thermal resistance to 370.2 K/W, resulting in the best heat dissipation. Because the heat dissipation performance is the main factor affecting device performance under high current, the device with diamond current confinement layer achieves the highest thermal roll-over current and output power. By utilizing diamond to replace SiO_2 as the current confinement layer, the output power is increased from 0.75 to 1.3 mW (an improvement of 73.3%), while the thermal roll-over current is increased from 42.3 to 80.1 mA (an improvement of 89.4%). As for the threshold current, on the other hand, the lowest value is achieved with the AlN confinement layer. These results provide a reference for selecting the materials of the current confinement layer in GaN-based VCSELs and are valuable for the design of high-performance GaN-based VCSELs.

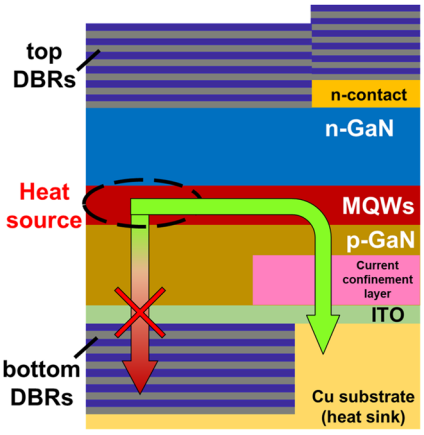

FIG. 1. Pathway of thermal transport inside the device.

II. DEVICE SIMULATION AND DISCUSSION

For the simulation, the devices were designed based on our previous studies,[8,29] as illustrated in Fig. 2(a). The devices with the SiO_2, AlN, and diamond current confinement layer are defined as device-SiO_2, device-AlN, and device-diamond, respectively. The studied VCSELs have a cavity sandwiched by a bottom 12.5 periods and a top six periods of Ta_2O_5/SiO_2 DBR. The cavity comprises a 944 nm-thick n-GaN layer, four pairs of $In_{0.28}Ga_{0.72}N$/GaN (2 nm/4 nm) multiple quantum wells (QWs), a 15 nm-thick p-type $Al_{0.2}Ga_{0.8}N$ electron blocking layer (p-EBL), and a 106 nm-thick p-type GaN layer. The VCSELs have a circular confinement aperture with a radius of 2.5 μm. Moreover, a 20 nm-thick Indium Tin Oxide (ITO) layer is utilized as the current spreading layer.[18]

As the positions of the active region and the ITO with respect to the standing wave significantly affect the optical performance of the VCSELs,[30] these layers are conserved in the same location in all structures to guarantee consistency of comparison in the simulation. The active region overlaps with the anti-node of the standing wave to maximize the modal gain, while the ITO layer overlaps with the node of the standing wave to reduce the absorption loss, as shown in Figs. 2(a) and 2(b). The emission wavelength of the devices is ~502 nm.

The investigations were conducted using PICS 3D[31] from Crosslight Software, and a self-consistent electro-opto-thermal simulation was adopted. The optical simulation was based on the

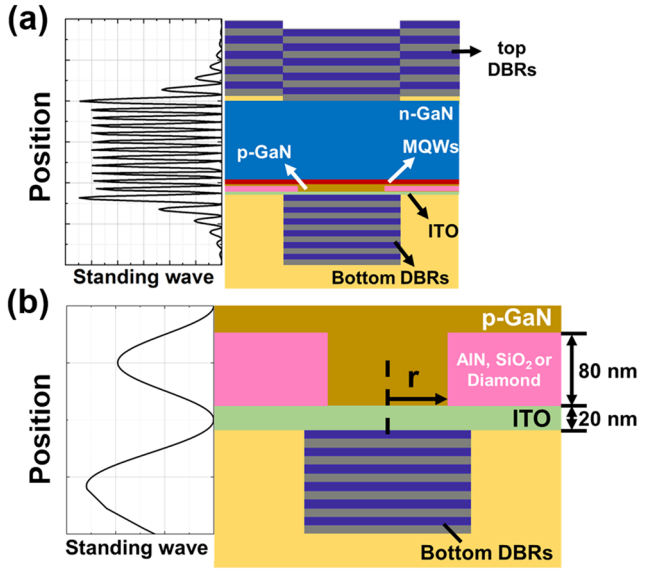

FIG. 2. (a) Structure and standing wave of VCESL. (b) The standing wave near the ITO region.

VCSEL Effective Index Method (VCSEL-EIM) approximation proposed by Hadley.[32–34] The optical modes within the VCSEL cavity were computed by solving the vector Helmholtz equation using a finite element method. The optical gain was calculated according to Fermi's Golden Rule.[35] In the electronic simulation, the band structure and bound carrier densities in strained quantum wells (QWs) were calculated by the k · p method with a 6 × 6 Hamiltonian for wurtzite materials.[36] The Poisson and Schrödinger equations were solved self-consistently in the active region considered the carrier screening. Furthermore, the charge transport in the bulk region was modeled with the drift-diffusion approximation.[37,38] In the thermal simulation, according to Mehta *et al.*,[24] the steady-state thermal diffusion equation for the lattice temperature is given by $Q = -\nabla \cdot \kappa \nabla T$, where Q, T, and κ are the heat generation density, the lattice temperature, and the thermal conductivity, respectively. Considering joule heat, recombination heat, and Thomson/Peltier heat as the heat sources, the heat generation density is given by

$$Q = \frac{\vec{j_n}^2}{\mu_n n q} + \frac{\vec{j_p}^2}{\mu_p p q} + qR_{nonrad}(\phi_p - \phi_n + T(P_p - P_n)) - \vec{J_n} \cdot T\nabla P_n - \vec{J_p} \cdot T\nabla P_p,$$

where the subscripts n and p refer to the quantity of electrons and holes, respectively. J, μ, and n (or p) are the carrier densities, mobility, and concentration. R_{nonrad} is the net rate of nonradiative recombination. ϕ_n and ϕ_p are the electron and hole quasi-Fermi potentials, and P is the thermoelectric power. The first two terms relate to Joule heating, and the third term describes the heating effect caused by nonradiative recombination throughout the device. The last two terms account for Thomson and Peltier heat. Further description of the electro-opto-thermal simulation method can be found in Refs. 39–41 and the references therein. Furthermore, the polarization level was set to 40%, meaning that 60% of the theoretical polarization induced charges are released by producing dislocations due to the strain relaxation during the epitaxial growth.[42] The band-offset ratio, which is defined as the ratio between the conduction-band offset and the valence-band offset for GaN/InGaN quantum wells, was set to 0.7/0.3.[43]

As the p-side of the devices was in direct contact with the copper substrate, they were assumed to link with a heat sink with high thermal conductivity (copper ~ 400 W/mK)[28] during the simulation. The current and the voltage were set to 5 mA and 4.7 V, respectively, so the input electrical power value was equal to 23.5 mW. The temperature distribution inside device-SiO_2 and device-AlN is shown in Figs. 3(a) and 3(b), respectively. The temperature rise was found to be 16.9 and 10.3 K, and the thermal resistance was calculated and was equal to 719.15 and 438.3 K/W for device-SiO_2 and device-AlN, respectively. These results prove that the AlN current confinement layer allows more efficient heat dissipation than SiO_2, with an improvement of 39%, which is consistent with our previous experimental results.[27] As the behavior of device-diamond shows in Fig. 3(c), the temperature rises and the thermal resistance of device-diamond was calculated to be 8.7 K and 370.2 K/W, respectively. The thermal resistance of device-diamond shows a 16% reduction compared to device-AlN. It means that the current confinement layer formed by diamond can further improve the heat transfer efficiency within the device.

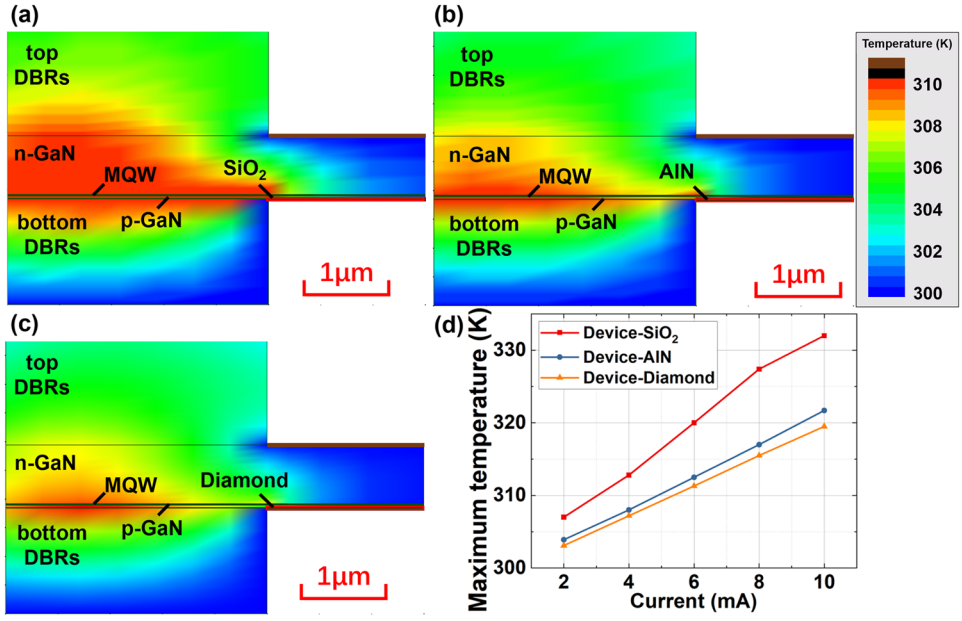

FIG. 3. Temperature distribution inside the (a) device-SiO_2, (b) device-AlN, (c) device-diamond at a current of 5 mA and an aperture radius r = 2.5 μm, (d) Maximum temperature inside the device in terms of the injection current.

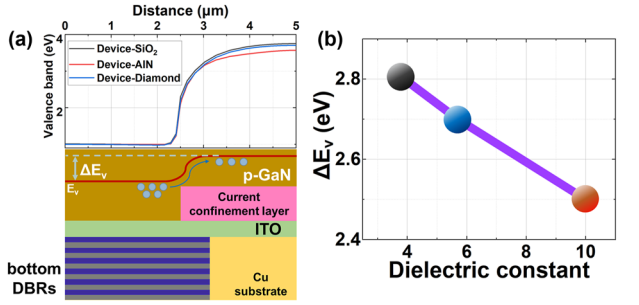

FIG. 4. (a) Lateral valence band diagrams in the p-GaN above the current confinement layer at a current of 5 mA. (b) Relationship between the dielectric constant and ΔE_v.

The maximum temperature variation with respect to the injection current is shown in Fig. 3(d), where, under the same current, the maximum temperature inside device-SiO_2, device-AlN, and device-diamond is sequentially decreasing. At the current of 10 mA, the maximum temperature for the three devices is 332, 321.7, and 319.5 K, respectively. Furthermore, the increasing rate of the maximum temperature decreases as the thermal conductivity of the current confinement layer increases (device-SiO_2 ~ 3.13 K/mA; device-AlN ~ 2.23 K/mA; device-diamond ~ 1.64 K/mA). Those results show that utilizing the diamond current confinement layer can realize the greatest heat dissipation performance.

Considering the purpose of current confinement, it is necessary to compare the current confinement capability of the different current confinement layers. According to Hang *et al.*,[44] as the current confinement layer consumes bias voltage during the device operation, a potential difference for the injected carriers appears between the inside and the outside of the aperture, which causes an energy bending of the band diagram inside p-GaN along the radial direction. The band bending favors the hole transport from the inside to the outside of the aperture, leading to the degeneration of the current confinement capability. Such band bending decreases with the increase of the dielectric constant of the current confinement layer. The leakage of the holes can be mitigated when a confinement layer with a higher dielectric constant is used.

As the dielectric constant of AlN is higher than that of diamond and SiO_2 (AlN ~ 10; diamond ~ 5.7; SiO_2 ~ 3.9), the band bending in device-AlN is expected to be smaller than that in device-SiO_2 and device-diamond. The lateral valence band profiles in the devices were calculated and shown in Fig. 4. Here, ΔE_v is defined as the energy barrier height in the valence band. As shown in Fig. 4, ΔE_v decreases as the dielectric constant of the current confinement layer increases. Figure 4(b) shows detailed information regarding the relationship between the dielectric constant of the current confinement layer and ΔE_v.

As discussed above, the current confinement capability of device-AlN is expected to be better than device-diamond and device-SiO_2. The hole concentration and the recombination rate at 5 mA were calculated to prove this point further. Figure 5(a) represents the lateral hole concentration in the p-GaN layer above the current confinement layer, and Figs. 5(b) and 5(c) show the longitudinal hole concentration and recombination rate in the active region, respectively. The vertical distribution of the hole in the active region shows a non-uniform distribution, which is caused by the low hole mobility.[45–48] The non-uniform distribution of carriers may impair the rate of stimulated radiation recombination in the n-side well, and adjusting the parameter of the QWs is a potential approach to improve uniformity. As shown in Fig. 5(a), the hole accumulation in the aperture of the three devices decreases in the following sequence: device-AlN (42.73×10^{16} cm^{-3}), device-diamond (35.65×10^{16} cm^{-3}), and device-SiO_2 (29.84×10^{16} cm^{-3}). The longitudinal hole concentration in the active region of the three devices decreased with a similar sequence, as shown in Fig. 5(b). The maximum hole concentration inside the last QW next to the p-type layer of device-AlN, device-diamond, and device-SiO_2 is 66.83×10^{18}, 64.29×10^{18}, and 60.71×10^{18} cm^{-3}, respectively. The recombination rate of the three devices also shows a similar sequence because the recombination rate is directly proportional to the concentration of the hole. The maximum recombination rate inside the last QW next to the p-type layer in device-AlN, device-diamond, and device-SiO_2 is 3.72×10^{28}, 3.53×10^{28}, and 3.24×10^{28} cm^{-3}, respectively. These results show that a better lateral current confinement capability and enhanced recombination can be

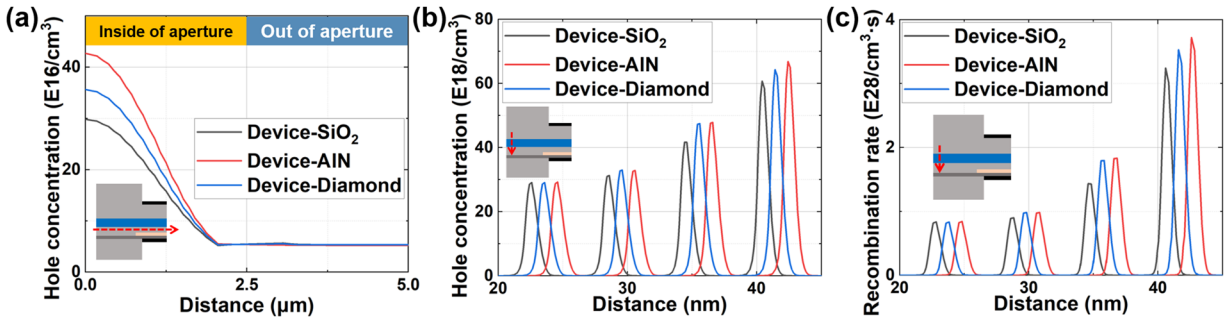

FIG. 5. (a) Lateral hole concentration, (b) longitudinal hole concentration, and (c) longitudinal recombination rate profiles along the marked positions for the inset schematic VCSEL at a current of 5 mA and an aperture radius of r = 2.5 μm.

obtained as the dielectric constant for the current confinement layer increases.

The optical output characteristics of the VCSELs were calculated after considering the above factors. The light-current characteristics for device-SiO_2, device-AlN, and device-diamond are shown in Fig. 6, and the threshold current, thermal roll-over current, and maximum output power are shown in Table I, the threshold current of device-SiO_2 was estimated to be 35.7 kA/cm^2, which is the same level of magnitude as the reported green GaN-based VCSEL.[49] The threshold current of device-AlN is the lowest. The reason is that under low injection current, the temperature is not very high to degrade the performance of the devices, and the lateral current confinement capability plays a critical role instead of the heat dissipation. As the injection current increases further beyond the threshold current, heat dissipation becomes the main factor affecting device performance. Since device-diamond has a smaller thermal resistance, the output power exceeds that of device-AlN under high injection current, showing the highest thermal roll-over current and largest output power among the three devices. By utilizing diamond to replace SiO_2 as the current confinement layer, the optical output characteristics are improved significantly, the output power is increased by 73.3%, and the thermal roll-over current is increased by 89.4%. Therefore, from the perspective of obtaining the high-power device, diamond is a better candidate than AlN and SiO_2 for the current confinement layer.

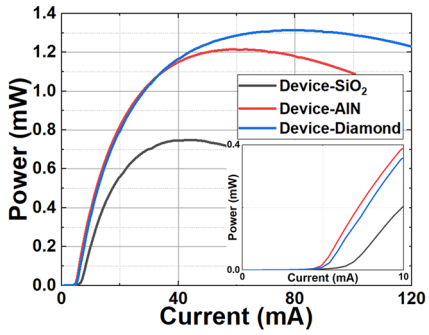

FIG. 6. Light-current characteristics of the device-SiO_2, device-AlN, and device-diamond.

TABLE I. Thermal roll-over current, maximum output power, and threshold current of the device-SiO_2, device-AlN, and device-diamond.

Device	Device-SiO_2	Device-AlN	Device-diamond
Threshold current (mA)	7	5.1	5.5
Thermal roll-over current (mA)	42.3	60.9	80.1
Maximum output power (mW)	0.75	1.2	1.3

III. CONCLUSIONS

In summary, this study investigated the performance of GaN-based VCSELs with different insulating materials. The results show that by utilizing diamond as the current confinement layer, the device can operate under a higher injection current without degradation and achieve a larger output power. This study on the current confinement layer provides a guide for developing high-power GaN-based VCSELs.

ACKNOWLEDGMENTS

This work was supported by the National Key Research and Development Program of China (Grant No. 2017YFE0131500), the National Natural Science Foundation of China (Grant Nos. 62104204, 62174140, 62234011, and U21A20493), and the President's Foundation of Xiamen University (Grant No. 20720220108).

AUTHOR DECLARATIONS

Conflict of Interest

The authors have no conflicts to disclose.

Author Contributions

Yan-Hui Chen: Conceptualization (equal); Data curation (equal); Formal analysis (equal); Investigation (equal); Methodology (equal); Validation (equal); Writing – original draft (equal); Writing – review & editing (equal). **Yang Mei**: Conceptualization (equal); Writing – review & editing (equal). **Zhong-Ming Zheng**: Writing – review & editing (equal). **Rong-Bin Xu**: Writing – review & editing (equal). **Ya-Chao Wang**: Writing – review & editing (equal). **Lei-Ying Ying**: Writing – review & editing (equal). **Zhi-Wei Zheng**: Writing – review & editing (equal). **Hao Long**: Writing – review & editing (equal). **Yi-Kun Bu**: Writing – review & editing (equal). **Bao-Ping Zhang**: Conceptualization (equal); Formal analysis (equal); Writing – review & editing (equal).

DATA AVAILABILITY

The data that support the findings of this study are available from the corresponding authors upon reasonable request.

REFERENCES

[1] T. Takeuchi, S. Kamiyama, M. Iwaya, and I. Akasaki, "GaN-based vertical-cavity surface-emitting lasers with AlInN/GaN distributed Bragg reflectors," Rep. Prog. Phys. **82**(1), 012502 (2019).
[2] H.-C. Yu, Z.-W. Zheng, Y. Mei, R.-B. Xu, J.-P. Liu, H. Yang, B.-P. Zhang, T.-C. Lu, and H.-C. Kuo, "Progress and prospects of GaN-based VCSEL from near UV to green emission," Prog. Quantum Electron. **57**, 1–19 (2018).
[3] M. Dummer, K. Johnson, S. Rothwell, K. Tatah, and M. K. Hibbs-Brenner, in *Optical Interconnects XXI*, edited by H. Schröder and R. T. Chen (SPIE, USA, 2021), p. 9.
[4] S. Sangu, T. Shimokawa, and S. Tanaka, in SPIE Augmented, Virtual, and Mixed Reality Conference, San Francisco, CA, edited by B. C. Kress and C. Peroz (SPIE, 2020), p. 50.

[5]G. Weng, Y. Mei, J. Liu, W. Hofmann, L. Ying, J. Zhang, Y. Bu, Z. Li, H. Yang, and B. Zhang, "Low threshold continuous-wave lasing of yellow-green InGaN-QD vertical-cavity surface-emitting lasers," Opt. Express **24**(14), 15546 (2016).
[6]T. Hamaguchi, Y. Hoshina, K. Hayashi, M. Tanaka, M. Ito, M. Ohara, T. Jyoukawa, N. Kobayashi, H. Watanabe, M. Yokozeki, R. Koda, and K. Yanashima, "Room-temperature continuous-wave operation of green vertical-cavity surface-emitting lasers with a curved mirror fabricated on {20−21} semi-polar GaN," Appl. Phys. Express **13**(4), 041002 (2020).
[7]J. T. Leonard, E. C. Young, B. P. Yonkee, D. A. Cohen, C. Shen, T. Margalith, T. K. Ng, S. P. DenBaars, B. S. Ooi, J. S. Speck, and S. Nakamura, in *Gallium Nitride Materials and Devices XI Conferences*, San Francisco, CA, edited by J.-I. Chyi, H. Fujioka, H. Morkoc, Y. Nanish, U. T. Schwarz, and J.-I. Shim (SPIE, 2016), p. 97481B.
[8]R. Xu, Y. Mei, H. Xu, L.-Y. Ying, Z. Zheng, H. Long, D. Zhang, B. Zhang, and J. Liu, "Green vertical-cavity surface-emitting lasers based on combination of blue-emitting quantum wells and cavity-enhanced recombination," IEEE Trans. Electron Devices **65**(10), 4401–4406 (2018).
[9]G. Weng, S. Chen, Y. Mei, Y. Liu, H. Akiyama, X. Hu, J. Liu, B. Zhang, and J. Chu, "Multiwavelength GaN-based surface-emitting lasers and their design principles," Ann. Phys. **532**(1), 1900308 (2020).
[10]T. Ide, R. Iida, T. Takeuchi, X.-L. Wang, N. Takada, and M. Shimizu, "Dynamic characteristics and device degradation of GaN-based vertical-cavity surface-emitting laser with an AlInN/GaN distributed Bragg reflector," Jpn. J. Appl. Phys. **60**(SB), SBBE01 (2021).
[11]P. S. Yeh, C.-C. Chang, Y.-T. Chen, D.-W. Lin, J.-S. Liou, C. C. Wu, J. H. He, and H.-C. Kuo, "GaN-based vertical-cavity surface emitting lasers with sub-milliamp threshold and small divergence angle," Appl. Phys. Lett. **109**(24), 241103 (2016).
[12]Y. Mei, G.-E. Weng, B.-P. Zhang, J.-P. Liu, W. Hofmann, L.-Y. Ying, J.-Y. Zhang, Z.-C. Li, H. Yang, and H.-C. Kuo, "Quantum dot vertical-cavity surface-emitting lasers covering the 'green gap,'" Light Sci. Appl. **6**(1), e16199 (2017).
[13]R. Iida, Y. Ueshima, W. Muranaga, S. Iwayama, T. Takeuchi, S. Kamiyama, M. Iwaya, and I. Akasaki, "GaN-based vertical cavity surface emitting lasers with lateral optical confinements and conducting distributed Bragg reflectors," Jpn. J. Appl. Phys. **59**(SG), SGGE08 (2020).
[14]C.-Y. Huang, K.-B. Hong, Z.-T. Huang, W.-H. Hsieh, W.-H. Huang, and T.-C. Lu, "Challenges and advancement of blue III-nitride vertical-cavity surface-emitting lasers," Micromachines **12**(6), 676–695 (2021).
[15]S.-M. Lee and D. G. Cahill, "Heat transport in thin dielectric films," J. Appl. Phys. **81**(6), 2590–2595 (1997).
[16]D. G. Cahill and T. H. Allen, "Thermal conductivity of sputtered and evaporated SiO_2 and TiO_2 optical coatings," Appl. Phys. Lett. **65**(3), 309–311 (1994).
[17]S. Orain, Y. Scudeller, and T. Brousse, "Thermal conductivity of ZrO thin films," Int. J. Therm. Sci. **39**(4), 537–543 (2000).
[18]Y. Mei, R.-B. Xu, H. Xu, L.-Y. Ying, Z.-W. Zheng, B.-P. Zhang, M. Li, and J. Zhang, "A comparative study of thermal characteristics of GaN-based VCSELs with three different typical structures," Semicond. Sci. Technol. **33**(1), 015016 (2018).
[19]W. J. Liu, X. L. Hu, L. Y. Ying, S. Q. Chen, J. Y. Zhang, H. Akiyama, Z. P. Cai, and B. P. Zhang, "On the importance of cavity-length and heat dissipation in GaN-based vertical-cavity surface-emitting lasers," Sci. Rep. **5**(1), 9600 (2015).
[20]G. Chen, "A comparative study on the thermal characteristics of vertical-cavity surface-emitting lasers," J. Appl. Phys. **77**(9), 4251–4258 (1995).
[21]M. Osinski and W. Nakwaski, "Thermal analysis of closely-packed two-dimensional etched-well surface-emitting laser arrays," IEEE J. Sel. Top. Quantum Electron. **1**(2), 681–696 (1995).
[22]R. P. Sarzala, P. Spiewak, and M. Wasiak, "Influence of resonator length on performance of nitride TJ VCSEL," IEEE J. Quantum Electron. **55**(6), 2400509–2400518 (2019).
[23]S. Mishkat-Ul-Masabih, J. Leonard, D. Cohen, S. Nakamura, and D. Feezell, "Techniques to reduce thermal resistance in flip-chip GaN-based VCSELs," Phys. Status Solidi A **214**(8), 1600819 (2017).
[24]K. Mehta, Y.-S. Liu, J. Wang, H. Jeong, T. Detchprohm, R. D. Dupuis, and P. D. Yoder, "Thermal design considerations for III-N vertical-cavity surface-emitting lasers using electro-opto-thermal numerical simulations," IEEE J. Quantum Electron. **55**(5), 2400308–2400316 (2019).
[25]J. T. Leonard, B. P. Yonkee, D. A. Cohen, L. Megalini, S. Lee, J. S. Speck, S. P. DenBaars, and S. Nakamura, "Nonpolar III-nitride vertical-cavity surface-emitting laser with a photoelectrochemically etched air-gap aperture," Appl. Phys. Lett. **108**(3), 031111 (2016).
[26]R. T. ElAfandy, J.-H. Kang, B. Li, T. K. Kim, J. S. Kwak, and J. Han, "Room-temperature operation of c-plane GaN vertical cavity surface emitting laser on conductive nanoporous distributed Bragg reflector," Appl. Phys. Lett. **117**(1), 011101 (2020).
[27]Y.-H. Chen, Y. Mei, H. Xu, R.-B. Xu, L.-Y. Ying, Z.-W. Zheng, H. Long, and B.-P. Zhang, "Improvement of thermal dissipation of GaN-based micro cavity light-emitting devices," IEEE Photonics Technol. Lett. **33**(1), 19–22 (2021).
[28]S. Kidalov and F. Shakhov, "Thermal conductivity of diamond composites," Materials **2**(4), 2467–2495 (2009).
[29]Y. Mei, R. Xu, L. Ying, J. Liu, Z. Zheng, H. Long, and B. Zhang, in *Gallium Nitride Materials and Devices XIV*, edited by H. Morkoç, H. Fujioka, and U. T. Schwarz (SPIE, San Francisco, USA, 2019), p. 52.
[30]P. Śpiewak, A. K. Sokół, M. Wasiak, and R. P. Sarzała, "Impact of AlN-aperture on optical and electrical properties of nitride VCSEL," Opt. Quantum Electron. **49**(3), 114 (2017).
[31]Crosslight Software, Inc., PICS 3D (Photonic Integrated Circuit Simulator in 3D), 2018.
[32]G. R. Hadley, "Effective index model for vertical-cavity surface-emitting lasers," Opt. Lett. **20**(13), 1483 (1995).
[33]G. R. Hadley, D. Botez, and L. J. Mawst, "Modal discrimination in leaky-mode (antiguided) arrays," IEEE J. Quantum Electron. **21**(4), 921–930 (1991).
[34]B. C. Lin, Y. A. Chang, K. J. Chen, C. H. Chiu, Z. Y. Li, Y. P. Lan, C. C. Lin, P. T. Lee, Y. K. Kuo, M. H. Shih, H. C. Kuo, T. C. Lu, and S. C. Wang, "Design and fabrication of a InGaN vertical-cavity surface-emitting laser with a composition-graded electron-blocking layer," Laser Phys. Lett. **11**(8), 085002 (2014).
[35]P. Blood, "On the dimensionality of optical absorption, gain, and recombination in quantum-confined structures," IEEE J. Quantum Electron. **36**(3), 354–362 (2000).
[36]S. L. Chuang and C. S. Chang, "A band-structure model of strained quantum-well wurtzite semiconductors," Semicond. Sci. Technol. **12**(3), 252–263 (1997).
[37]Y. Gao, C. Chu, S. Hang, Y. Zhang, Z.-H. Zhang, and J. Zhou, "Quantum barriers with a polarization self-screening effect for GaN-based VCSELs to increase the electron-hole stimulated recombination and output performance," Opt. Mater. Express **11**(12), 3984 (2021).
[38]Y.-Y. Lai, T.-C. Lu, T.-L. Ho, S.-C. Huang, and S.-C. Wang, in *Vertical-Cavity Surface-Emitting Lasers XVIII Conferences*, San Francisco, CA, edited by J. K. Guenter and C. Lei (SPIE, 2014), p. 90010J.
[39]K. Mehta and P. D. Yoder, "Philosophy of approaching a laser design problem: Illustrated by the design of ultraviolet vertical-cavity laser diodes," Phys. Status Solidi A **217**(18), 2000154 (2020).
[40]A. Tibaldi, F. Bertazzi, M. Goano, R. Michalzik, and P. Debernardi, "VENUS: A vertical-cavity surface-emitting laser electro-opto-thermal numerical simulator," IEEE J. Sel. Top. Quantum Electron. **25**(6), 1500212–1500224 (2019).
[41]P. Debernardi, A. Tibaldi, M. Daubenschuz, R. Michalzik, M. Goano, and F. Bertazzi, "Probing thermal effects in VCSELs by experiment-driven multiphysics modeling," IEEE J. Sel. Top. Quantum Electron. **25**(6), 1700914–1700928 (2019).
[42]Z.-H. Zhang, S. T. Tan, W. Liu, Z. Ju, K. Zheng, Z. Kyaw, Y. Ji, N. Hasanov, X. W. Sun, and H. V. Demir, "Improved InGaN/GaN light-emitting diodes with a p-GaN/n-GaN/p-GaN/n-GaN/p-GaN current-spreading layer," Opt. Express **21**(4), 4958 (2013).
[43]Y.-K. Kuo, B.-T. Liou, M.-L. Chen, S.-H. Yen, and C.-Y. Lin, "Effect of band-offset ratio on analysis of violet–blue InGaN laser characteristics," Opt. Commun. **231**(1–6), 395–402 (2004).
[44]S. Hang, Y. Zhang, Y. Gao, X. Qiu, J. Kou, K. Tian, and Z.-H. Zhang, "On the origin for the hole confinement into apertures for GaN-based VCSELs with buried dielectric insulators," Opt. Express **28**(6), 8668 (2020).
[45]H. Yamazaki, A. Tomita, M. Yamaguchi, and Y. Sasaki, "Evidence of nonuniform carrier distribution in multiple quantum well lasers," Appl. Phys. Lett. **71**(6), 767–769 (1997).

[46]D. C. Nguyen, D. Vaufrey, and M. Leroux, in *Fourteenth International Conference on Solid State Lighting and LED-based Illumination Systems*, San Diego, CA, SPIE, edited by M. H. Kane, J. Jiao, N. Dietz, and J.-J. Huang (SPIE, 2015), p. 95710J.
[47]S.-N. Lee, H.-Y. Ryu, H.-S. Paek, J.-K. Son, T. Sakong, T. Jang, Y.-J. Sung, K.-S. Kim, K.-H. Ha, O.-H. Nam, and Y. Park, "Inhomogeneity of InGaN quantum wells in GaN-based blue laser diodes," Phys. Status Solidi (c) **4**(7), 2788–2792 (2007).
[48]Y. Kuroiwa, Y.-I. Matsushita, K. Harada, and F. Oba, "Theoretical prediction of strain-induced carrier effective mass modulation in 4H-SiC and GaN," Appl. Phys. Lett. **115**(11), 112102 (2019).
[49]D. Kasahara, D. Morita, T. Kosugi, K. Nakagawa, J. Kawamata, Y. Higuchi, H. Matsumura, and T. Mukai, "Demonstration of blue and green GaN-based vertical-cavity surface-emitting lasers by current injection at room temperature," Appl. Phys. Express **4**(7), 072103 (2011).